12-13-2000

Thermoelectric Single-Photon Detectors for X-Ray/UV Radiation

G. G. Fritz
Naval Research Laboratory

K. S. Wood
Naval Research Laboratory

D. Van Vechten
U.S. Office of Naval Research

A. L. Gyulamiryan
National Academy of Sciences of Armenia

A. S. Kuzanyan
National Academy of Sciences of Armenia

See next page for additional authors

Recommended Citation

Fritz G.G., Wood K.S., Van Vechten D., Gyulamiryan A.L., Kuzanyan A.S., Giordano N.J., Jacobs T.M., Wu H.-D., Horwitz J.S., and Gulian A.M., Thermoelectric single-photon detectors for X-ray/UV radiation. *Proc. SPIE*, 2000, vol. **4140**, pp. 459-469. https://doi.org/10.1117/12.409144

Thermoelectric Single-Photon Detectors for X-Ray/UV Radiation

Authors

G. G. Fritz, K. S. Wood, D. Van Vechten, A. L. Gyulamiryan, A. S. Kuzanyan, N. J. Giordano, T. M. Jacobs, H.-D. Wu, J. S. Horwitz, and Armen Gulian

Thermoelectric single-photon detectors for X-ray/UV radiation

G. G. Fritz[a], K. S. Wood[a], D. Van Vechten[b], A. L. Gyulamiryan[c], A. S. Kuzanyan[c]; N. J. Giordano[d], T. M. Jacobs[d], H.-D. Wu[a], J. S. Horwitz[a], A. M. Gulian[e]

[a]Naval Research Laboratory, Washington, DC 20375

[b]Office of Naval Research, Arlington, VA 22217

[c]Physics Research Institute, National Academy of Sciences, Ashtarak-2, 378410, Armenia

[d]Department of Physics, Purdue University, West Lafayette, IN 47907

[e]USRA/Naval Research Laboratory, Washington, DC 20375

ABSTRACT

A feasibility study of megapixel microcalorimeter arrays, based on thermoelectric energy to voltage conversion and digital superconducting readout, is presented. The design concept originated from the philosophy of employing the simplest principles at the single-pixel level to enable large arrays without sacrificing energy resolution, fast operation speed, and quantum efficiency. Initial experimental tests confirm the basic predictions of theory, and show no major obstacle in achieving the desired characteristics.

Keywords: imaging microcalorimeter, energy resolution, thermoelectric sensors, hexaborates.

1. INTRODUCTION

At the frontiers of celestial X-ray/UV astronomy, two aspects of the instrumentation will determine the ultimate limitation on future missions. The first is the effective area of the mirror or mirror equivalent. Improvements in spatial, spectral, temporal, or other resolution must be accompanied by increased numbers of source photons to maintain adequate statistics and thus signal-to-noise for the signal features under study. The second critical aspect is the efficiency and spectral resolution of the detector. Modern CCD detectors have already achieved efficiencies in excess of 90% of their theoretical limit with excellent spatial resolution, but are limited in their temporal resolution by the long read-out time per pixel. More importantly, their non-dispersive spectral resolution is limited statistically so that ΔE_{FWHM} cannot exceed the level of ~100 eV for E=6 KeV photon events. Although incremental improvements will certainly continue to be made, obtaining a large increase in detector capabilities requires a new detector paradigm.

The next generation of single-photon detectors will need to be hyperspectral imaging detectors capable of obtaining high spectral resolutions (up to $E/\Delta E_{FWHM}$=10,000 for E=1–6 KeV x-ray photon events and $\lambda/\Delta\lambda$ >100 for UV photons) and processing high event rates, while maintaining high spatial resolution and high focal plane efficiency. We are developing the QVD detector, a hyperspectral replacement for the CCD which would represent a revolutionary increase in capability for future NASA missions and would contribute to NASA's "Origins" and "Cosmic Journeys" programs. The QVD detector is an array of photon counting pixels, each of which absorbs incoming photons, converts the photon energy to heat (Q), thermoelectrically converts the heat to a voltage (V), and then processes the voltage pulse into a digital (D) signal. Each QVD pixel contains an absorber and a heat sink coupled by a thermoelectric sensor. When a photon is absorbed, the absorber becomes warmer than the heat sink. The heat flowing from the absorber to the heat sink through the sensor generates a Seebeck voltage across the sensor without an external bias voltage or current. This voltage is read out by cryogenic electronics devoted entirely to the absorber-heat sink pair; the voltage pulse is processed into a digital measure of the energy deposited in the absorber and stored in an on-chip memory. A separate circuit is used to sequentially read out the pixel array.

X-Ray and Gamma-Ray Instrumentation for Astronomy XI, Kathryn A. Flanagan, Oswald H. W. Siegmund, Editors, Proceedings of SPIE Vol. 4140 (2000) © 2000 SPIE · 0277-786X/00/$15.00

By mutiplexing the digital data, a single, easily connected optical fiber can deliver data from 1000 pixels at frame rates up to 1 MHz.

The QVD detector enjoys a number of significant advantages over other hyperspectral detectors and detector concepts, most notably microcalorimeter and microbolometer arrays using either superconducting tunnel junction (STJ) or transition edge sensor (TES) technologies. The QVD sensors need no applied biasing. The single thermoelectric sensor used to read out each absorber-heat sink pair means that only one low current lead is required per pixel. This greatly simplifies the complexity of array wiring over other concepts and facilitates the vertical packaging which is a key feature of the QVD readout concept. High spatial resolution (10-20 μm scale pixels) and high focal plane area efficiency (>90% due to the small dead space between pixels) naturally result from this simplification.

Most groups working in the area of microcalorimeters and other hyperspectral pixel array detectors have begun with fairly well developed single pixel concepts and then have struggled with varying degrees of success to identify a realistic array concept which incorporates a useable readout system. We begin with a well developed read out system, and a concept for single pixel detectors that are easily and naturally placed into a large format array. In this report, we discuss the demonstration of the fundamental operational aspects of the QVD detector by developing prototype basic pixels. The basic physics involved dates back to the discovery of Seebeck voltages in 1823, and it has been used for reliable temperature measurements in other applications for decades.

2. QVD CONCEPT

Figures 1 and 2 elucidate the operational principle of the thermoelectric sensor, which is the primary component of the QVD device.

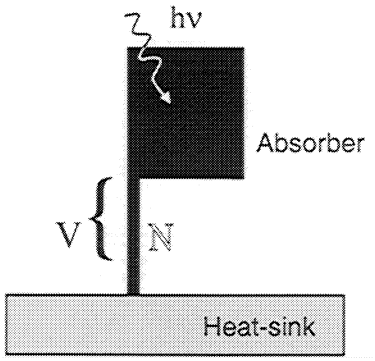

Figure 1. Absorption of the photon by a normal-metal film elevates its electronic temperature. Electrons flow out through the normal-metal lead (N) and create a voltage V measurable between the absorber and heat-sink. This voltage is called the Seebeck voltage.

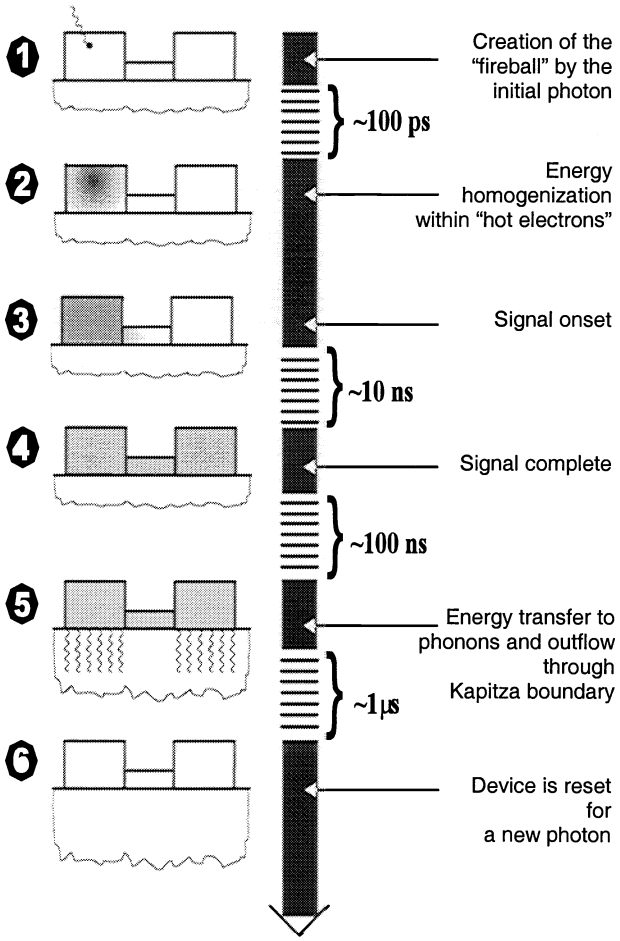

Figure 2. Operational circle of thermoelectric detector. Energy thermalization and subsequent homogenization within a metallic film is a very fast process. For typical cases it is less than 100 ps. In the configuration shown here, signal duration is equal to the time of energy homogenization between the left and right identical units. This time is about 10-20 ns for typical devices. Because of Kapitza resistance between metals and the dielectric substrate, the heat outflow (resetting) time is much longer, about 1μs.

The central driving concept is to use a thermoelectric thermometer in a microbolometer. One can only speculate why no serious consideration was devoted to this type of temperature measurement in earlier microbolometric research. It may have been because common thermoelectric thermometers (say, Au with 0.07% of Fe impurities) were developed to have a monotonic response in a wide temperature range and thus are not outstanding in sensitivity. We are optimizing the thermoelectric sensors for a narrow range 0.1-1 K and are able to chose materials with much higher sensitivity.

3. EXPERIMENTAL PROGRESS AND STATUS

Prior to 1999 our experiments had focused on understanding and proving that the response of *anisotropic* materials to light pulses is a thermoelectric response [1] and that it could be used as the basis of an energy resolving photon detector [2]. We had also completed a literature survey which showed that the only known materials with large low temperature Seebeck (thermoelectric) coefficients are *isotropic*. We then used our understanding of sensor operation to redesign the device to utilize the response of isotropic materials. That required a total change in the device layout. Thus one year ago we had a well-precedented design, but no experimental results on devices we hoped to develop further.

Our first effort to test an isotropic QVD sensor occurred in August 1999 using a device made by crudely modifying a structure originally fabricated for another purpose. It achieved an energy resolution of ~150 KeV when exposed to pulses of UV radiation (millions of photons per pulse). Shown in Fig. 3a, this device consisted of a small 30μm high triangle 0.5 μm thick Au absorber, and a larger triangle (150 μm high) that is a heat-sink. The absorber and heat-sink are connected by a Au + 100 ppm Fe sensor (too small to be visible in this figure). Rough silver glue pads were used for electric leads; these leads seriously reduced the performance of this first device.

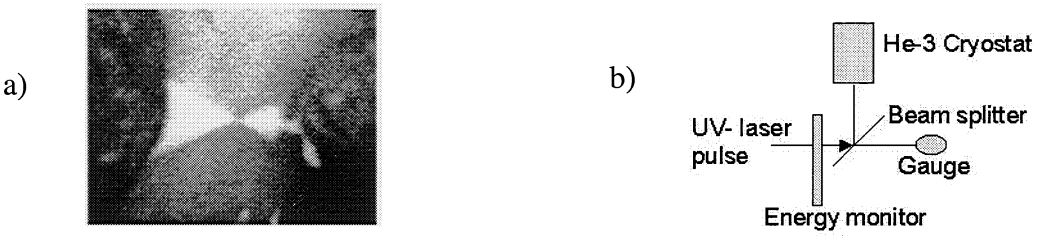

Figure 3. a) The first prototype used to demonstrate the biasless QV-transformation (August 1999); b) experimental scheme.

The second generation of devices attained an energy resolution of 1.5 KeV at 6 KeV in October 1999 (shown with its leads and contact pads in Fig. 4. These devices had a 18×22×0.2 μm Sb absorber, an identical heat-sink, and a 2×26×0.5 μm sensor made of the same Au + 100 ppm Fe as the first generation device. The use of superconducting Sn electric leads and Sb absorber/heat sink led to the factor of 100 improvement in performance. As in the previous generation, the laser pulses were shining homogeneously onto the device, the second half of which (the heat sink) was shadowed by foil.

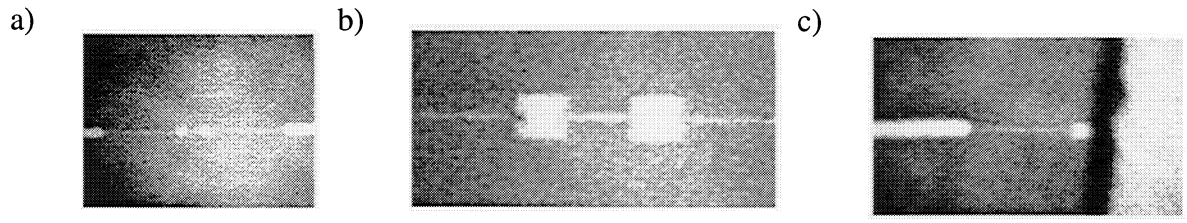

Figure 4. The prototype device. a) Wide Sn leads transform into narrow strips attaching the Sb absorber and heat-sink with an Au-Fe sensor between them; b) the central part of the device enlarged; c) shadowing the half of the device by a foil screen, right.

The third generation of devices uses a full set of photolithography masks and is made in fully integrated fashion by team members at NRL, with help from Purdue University. The custom designed masks for a 10x10 μm chip contain 32 devices (Fig. 5). The devices on each chip systematically vary a single parameter at a time to allow an empirical search for the optimum configuration.

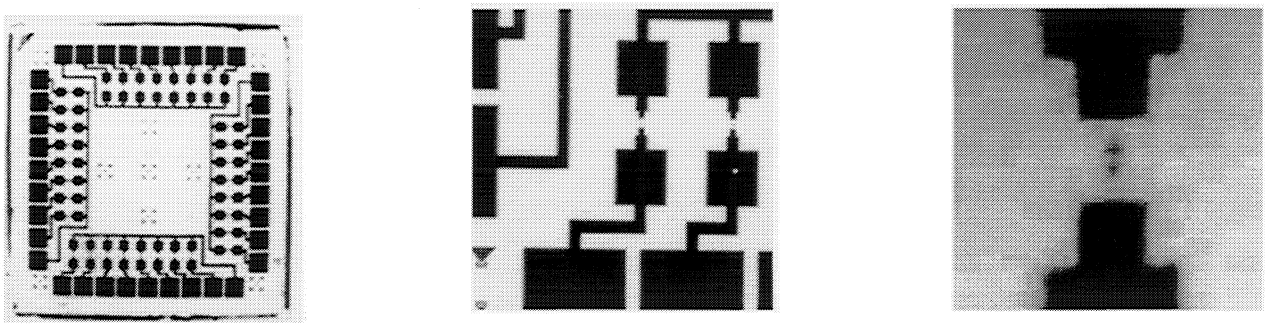

Figure 5. Devices produced for systematic experimental search for the best design parameters. (a) General layout: 4 groups of 8 devices with a common lead, only one parameter is changed in one group; (b) the lead structure enlarged, device is not visible on this scale and is shown in (c).

The first samples from this mask provided an object lesson in the importance of close collaboration between the device fabricators and device developers. The devices displayed no response at all when first run. We now understand that this is due to an unanticipated fabrication issue – Cr cannot be used as an etch mask in the sensor definition phase[1]. It was not until we applied sufficient DC current (40 μA) to the sensor to drive superconducting Cr remnants into the normal state that a large response to light pulses appeared. Afterward, we found literature evidence [3] that Cr can become superconducting when ion beam sputtered with Ar, Kr, or Xe, with transition temperatures in the range 0.6-3.1 K.

This experience has reconfirmed our device model – had the Cr remained a normal metal, it would have reduced the signal amplitude but not eliminated it. This learning experience has cost "only" a few months of schedule delay. We are now investigating alternative etch masks and plan to fabricate more samples immediately.

We expect the current generation of Au-Fe sensor devices to provide energy resolution below 100 eV for 6 KeV incident, another factor of 15 improvement compared to the second generation. We show in the next Section that a further factor of 100 improvement is possible. That is, energy resolution of 1 eV or even less may be achievable.

4. TOWARD 1 eV RESOLUTION AND BEYOND

We have fully discussed the physics of the QVD detector at professional meetings of the detector and thermoelectricity communities (see Refs. [4,5] which summarize the arguments). Therefore the model presented there will be used here without derivation. Theoretically achievable *energy resolution* is determined by the signal-to-noise ratio, and for the structure shown in Fig. 4 can be expressed as:

$$\Delta E_{FWHM} = 2.35\{2k_B T^2 C_{abs}(1+L_0/S^2)\}^{1/2} \qquad (1)$$

Here C_{abs} is the absorber (and identically structured heat-sink) heat capacity, S is the Seebeck coefficient of the sensor, T is the bias temperature, and $L_0 = 25\ nW\Omega/K^2$ is the Lorenz number. The first term in braces is related to the thermal noise and the second to the Johnson noise. For example, at T~0.3K, C_{abs}~1fJ/K, S~100μV/K, one deduces E_{FWHM} ~1 eV. Even higher resolutions (~0.1 eV) are possible for smaller C_{abs}, lower temperatures and materials with higher values of S (see discussion in Section 4).

[1] In the fabrication step that defines the narrow sensor element, a robust etch mask is required. Cr is a standard choice and as deposited is a normal metal. However, even though an effort was made to fully remove the Cr by ion milling as the final fabrication step, enough remained that it formed a conductive coating. Moreover, thanks to the ion bombardment, it was converted into a superconductor with a transition temperature about 0.6 K (base temperature of the cryostat is 0.35K). When the coating became a superconductor below 0.6 K, it shorted out the device's thermoelectric response.

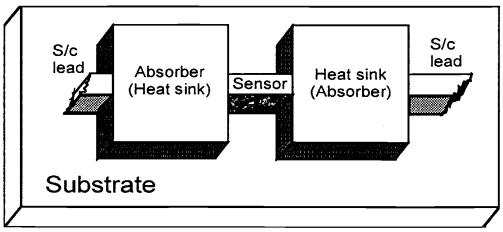

Figure 6. Conceptual schematic of double pixel structure, used in current experiments.

Thermoelectric sensors can function as either voltage or current sources. The low working temperatures and low impedance of the sensors facilitate using SQUIDs as preamps for the lowest noise. SQUIDs measure current and transform it into voltage (Fig. 7).

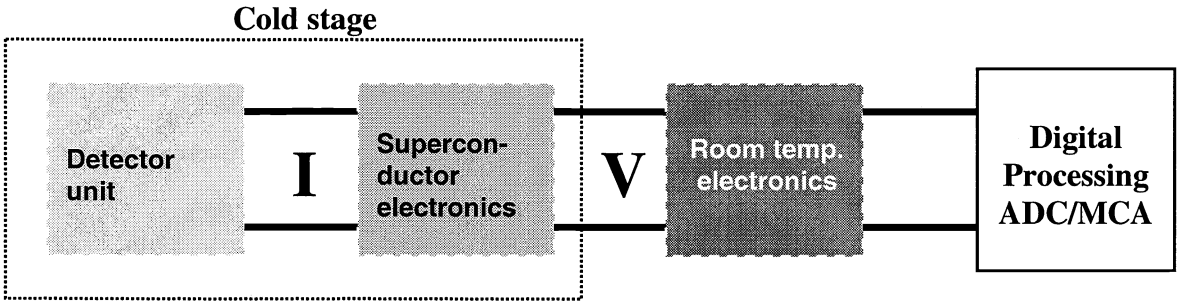

Figure 7. Signal acquisition scheme in single-pixel experiments.

Three important considerations about the signal chain are apparent from this scheme:

a) Any parasitic resistance should be eliminated (in devices, interconnections, etc.).

b) Input/output impedances should match in stage I, and in stage V, the amplifier input noise should be lower than the output noise level from the SQUID preamplifier.

c) Signal acquisition bandwidth should be optimized.

The 150,000 → 1,500 eV energy resolution improvement between our first and second generation devices was due not only to the device improvements, but also to our successful efforts to begin to address these factors. Our current samples (Fig.5) have $R_{det.unit}$ ~0.3 Ω, while the duration of the signal, shown in Fig.8, is not more than 50 ns.

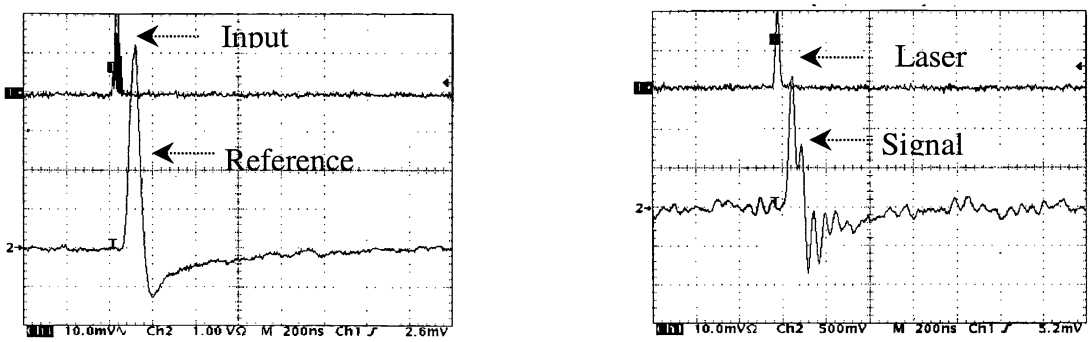

Figure 8. Test pulse (20ns duration) input and electronics response, left; photodiode (top) and QVD detector (bottom) response to laser pulse, right.

Given that $C_{abs} \cong 2$ fJ/K and T=0.65 K, this agrees with the model in Refs. [4 and 5]. There the signal duration is expressed as

$$\tau_{signal} = C_{abs}R/(L_0/T) \quad (2)$$

This predicts τ_{signal} should be about 15 ns, which means that the expected value of signal bandwidth is $\nu_B \sim$ 70 MHz and $\omega = 2\pi\nu_B = 4\times10^8\ s^{-1}$. The experiment confirms that ν_B is at least 50 MHz. Our SQUID amplifier had L=1/4 μH so its input impedance Z = Lω is not less than 30Ω and could have been as large as 100Ω. Comparing $R_{det.unit}$ and Z, we now understand we were losing 2 or more orders of magnitude in signal amplitude on stage "I" of Fig.5. We need a custom SQUID amplifier with smaller input inductance. Another (one) order of magnitude degradation of S/N is currently lost at the stage "V", since we used room temperature electronics with input noise ~2nV/Hz$^{1/2}$. We have more recently found a much better choice (~0.3nV/Hz$^{1/2}$ [6]). We have tested it in our lab, and it is clear that the electronics can be tuned in a rather straightforward manner to make the electronic noise lower than that of the device, as is assumed in Eq. (1). For this task we already have in hand SQUID amps with L=25 nH (made at TRW) with bandwidth more than 10 MHz. Though not yet ideal for 1 eV energy resolution, these values are good enough for the intermediate task. Currently the noise of the Au-Fe-device itself limits the achievable energy resolution to about 20 eV. Two orders of magnitude improvement in electronics performance is enough for these devices to reach their theoretical resolution. The third order of magnitude will require hexaborate sensor devices, which will eventually replace the current Au-Fe prototypes. We expect also to have available full custom electronics that matches the device requirements ideally. That will be the fourth generation of devices.

To understand the hexaborate sensor issue we present two plots in Fig. 9:

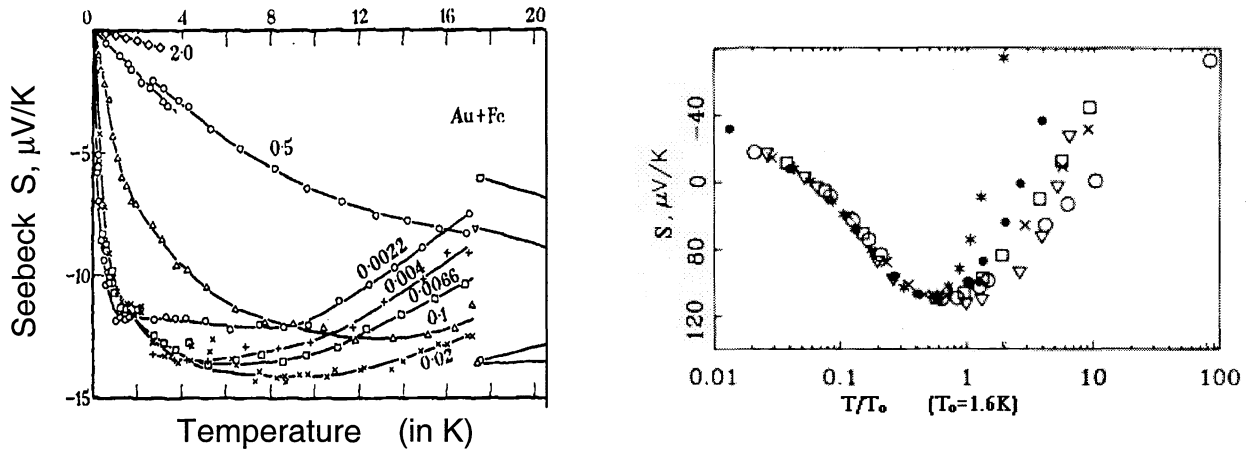

Figure 9. S in Kondo metals: left is Au+Fe [7] for different iron concentrations; right is La(Ce)B_6 [8] for different Ce concentrations.

Comparison of these plots indicates that hexaborates have about ten times larger values of the Seebeck coefficient than Au-Fe at the <1 K bias temperature required by thermal noise considerations. According to (1), this means that one will gain an order of magnitude in energy resolution by replacing the Au-Fe sensor with a La(Ce)B_6 sensor. Moreover, this material has about three times higher resistivity than Au-Fe, so according to (2), the duration of signal will be longer, the bandwidth ν_B will be lower, and the overall signal handling will be easier. One should bias the detector at about 300 mK, which is within the range for getting optimal values of S(T) using the hexaborate sensors (the temperature scale is logarithmic in Fig.9 for La(Ce)B_6). For such a bias temperature, C_{abs}=1/4 fJ/K absorbers would yield ΔE_{FWHM} =1 eV. A 6 KeV photon deposits about 1 fJ, so that to keep the temperature rise small (~1 K), C_{abs} ~ 1fJ/K is desirable. This size would still deliver a resolution ΔE_{FWHM} ~2 eV.

Development of lanthanum-cerium hexaborate thin film technology to replace the Au-Fe sensors in these devices and obtain the additional order of magnitude improvement in resolution is a challenging task, since the thin film technology for La(Ce)B_6 is not well developed. We have already started this research. As the diffractograms in Fig. 8 indicate, for

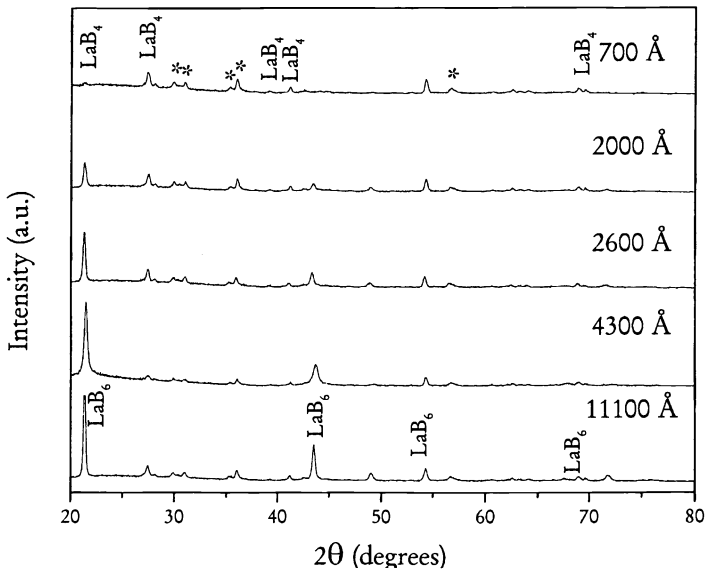

Figure 10. X-ray diffractograms of hexaborate films produced for proposed detectors. Unidentified peaks are denoted by (*). Samples are prepared by the collaborating group at Nat'l Acad. Sci., Armenia.

thick (~1 μm) films there is good phase structure. Two immediate tasks are: (a) further improve the quality of thin films (i.e., get rid of parasitic phases corresponding to unidentified peaks in Fig.10) and (b) confirm the existence of 1% of Ce in films. After completing these tasks one can start using the films in the device manufacturing. The third task is to check the electron-phonon lifetime for $La(Ce)B_6$. As we discussed above, in the properly designed device this parameter must be longer than the signal duration. There are no data for this material in the literature.

Our first measurement of Seebeck's coefficient in thin film samples is shown in Fig. 11.

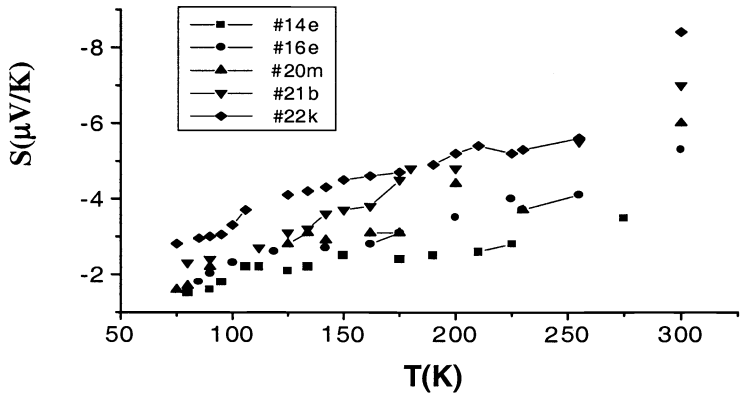

Figure 11. Measured values of S in $La(Ce)B_6$ thin films at T=77-300 K (samples and measurements were made by the collaborating group at Nat'l Acad. Sci., Armenia). Extrapolation of these curves towards lower temperatures indicates that (at least in some samples) S(T) changes its sign thus revealing the behavior plotted in Fig. 9 for bulk samples. The low temperature behavior of these thin film samples still should be studied.

Additional enhancement of energy resolution is possible by varying both the geometric sizes of the pixel and the absorber material and the bias temperature. Systematic comparison of the relevant properties of all the elemental materials

revealed that the best choice is Au or Sb for X-ray photons. For both materials data exists on the electron-phonon relaxation times. At 300 mK these times are $\tau_{e\text{-}ph}$~1.4-1.9 μs for Au and $\tau_{e\text{-}ph}$~ 0.27-2.7 μs for Sb [5]. They are much longer than the time required for the excess energy to become homogeneously distributed between the absorber and heat sink: less than 50 ns as was discussed in Fig.2. The heat is transferred in the form of "hot electrons", and they are alone responsible for the (thermoelectric) voltage signal. The phonons participate negligibly at this stage (see Table 1 for electron-phonon interaction times). The temperature rise following absorption of photons takes place in the electronic system.

Table 1. Electron-phonon interaction time, $\tau_{e\text{-}ph}$ in some metals*

metal	$\tau_{e\text{-}ph}$ @ 1 K [μsec]	$\tau_{e\text{-}ph}$ @ 0.3 K [μsec]
Ag	0.09-1.1	2.4-3.0
Au	0.05-0.07	1.4-1.9
W	0.05	0.5
Sb	0.01-0.1	0.27-2.7

*) $\tau_{e\text{-}ph}$ scales as $\propto T^{-3}$ for Ag, Au and Sb, and $\propto T^{-2}$ for W. The data are obtained by RFSE technique [10-13].

Thus one should take into account only the electronic contribution into C_{abs}. C_{abs} ~2 fJ/K transfers into a volume V_{abs}~ 100 μm^3 for Au-absorbers (see Table 2).

Table 2. Thermal parameters for candidate absorber metals*

metal, Z	$C_v^{el} = \gamma^{el} T$ @1 K [$\mu J\ cm^{-3} K^{-1}$]	C_v^{tot}, @1 K [$\mu J\ cm^{-3} K^{-1}$]	$C_v^{el} = \gamma^{el} T$ @0.3 K [$\mu J\ cm^{-3} K^{-1}$]	C_v^{tot}, @0.3 K [$\mu J\ cm^{-3} K^{-1}$]	V_{abs} yielding C_{abs}^{tot}= 1 fJ/K @0.3 K, [μm^3]
Be, 4	34-47	45	14	10-14	70-100
As, 33	14		4.2	>22.7	~40
Sb, 51	6-30		1.8-9	10-14	~100
Bi, 83	0.4-3	20	0.1-0.9	0.7-1.4	~1000
Au, 79	60-80	120	18-27	20-30	30-50
W, 74	140	140	40	40	25

*)The data were compiled and calculated using [14-16]. The very complicated character of the electron-phonon interaction, as well as the anisotropy causes the large uncertainty for the case of semi-metals As, Sb and Bi.

A detector unit with pixel size 10 μm×10 μm and thickness 1 μm will have energy resolution better than 3 eV for 6 KeV photons with a temperature excursion in the "hot electron" system of less than 0.5 K. As shown in Fig.9, such excursions will not take the device out of the effective operational temperature range. In the case of Sb-absorbers C_{abs} ~2 fJ/K means a volume V_{abs}~ 220-1200 μm^3 (Sb has a larger uncertainty in Sommerfeld's constant γ, $\gamma = C_{abs}/V_{abs}T$, and thus in the electronic heat capacity). The absorption of Sb is given in Table 3. Although at higher energies antimony has a smaller absorption

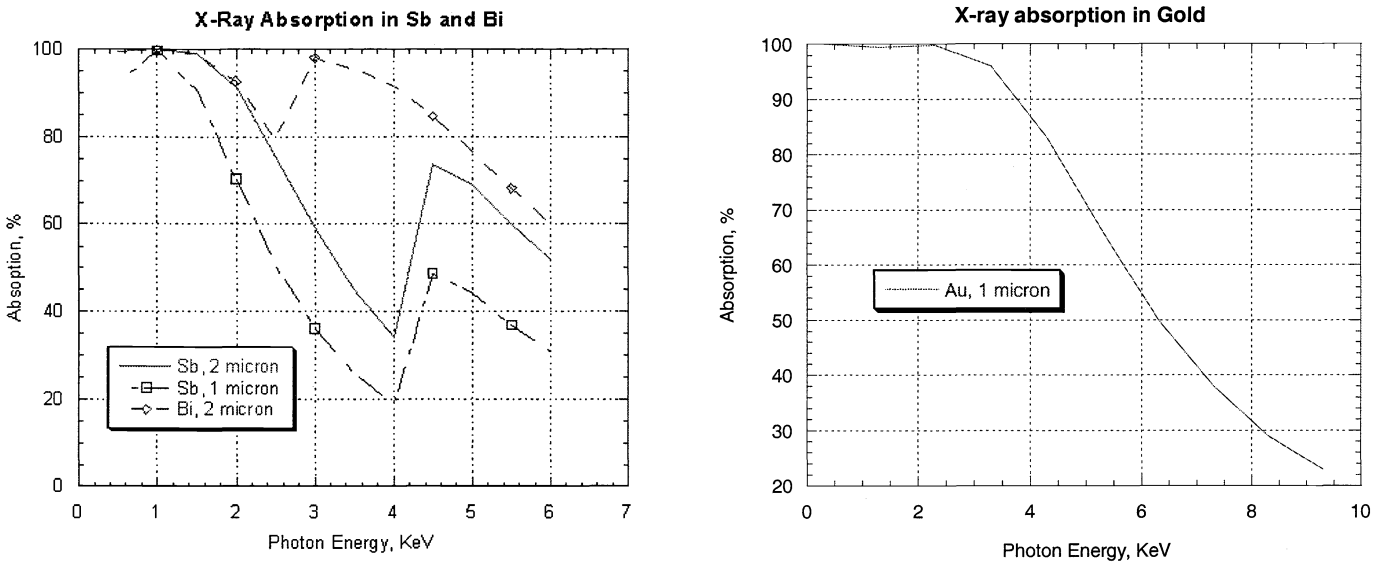

Figure12. Antimony, bismuth and gold as possible candidate materials for absorbers of QVD detector will have different quantum efficiencies, pixel sizes and energy resolutions (calculations by M. Kowalski, NRL Code 7620).

Table 3. Absorption efficiency of single UV/EUV photons in crystalline Sb films

Wavelength, Å	1000	500	33	25	20	17	14	12	11	10
Efficiency, % , at d = 0.25 μm	100	91.12	52.4	99.9	99.9	99.9	99.5	97.9	95.1	91.9
Efficiency, %, at d = 1 μm	100	99.99	94.87	100	100	100	100	100	99.9	99.9

coefficient than gold (see Fig. 12), and correspondingly, lower quantum efficiency at the same absorber thickness, it is suitable for low and intermediate energy photons and can provide larger pixel sizes at the same resolution level or higher resolution at the small pixel sizes. Bismuth is also a good candidate to test as an absorber: it has about 10 times lower heat capacity than Sb and thus can yield larger pixel sizes.

5. MEGAPIXEL ARRAYS AND DIGITAL READOUT

One of the great advantages of the QVD detector is that there is a clear development path from single-pixel devices to large arrays. This process is aided by the fact that thermoelectric detectors have a much larger signal bandwidth than that of the substrate-related phonon noise (see Fig.13). This differentiates the QVD approach from competing microcalorimeter devices, and allows our detectors to be placed directly on substrates, thus avoiding "pop-up" [9] or suspended structures, and permitting more rugged, edge mounted solid substrate structures (Fig.14). For example, for pixel sizes of 20 μm, 1000 pixels in a row can be placed on a thin wafer 2 cm in length, and up to 1000 of these wafers can be stacked to form a complete megapixel detector. In this arrangement, the electronics (amplification, A/D conversion, signal storage and readout) for an entire row can be integrated onto the side surface of the wafer, so that only a few external connections to one substrate are necessary. Noting that a single set of electronics serves for two pixels, it is instructive to estimate the surface area required for the electronics on a wafer (assumed to be 1000 pixels). A SQUID amplifier occupies about 100,000 μm^2, an A/D converter

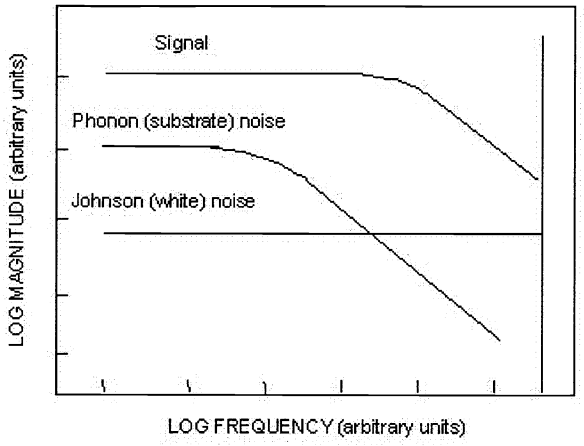

Figure 13. The characteristic time-scale for the energy exchange with substrate is set up by the Kapitza time: $\tau_K=r_0C_{abs}/T^3A_{abs}$ [4], (where r_0 = 20 K^4cm^2/W, and A_{abs} is substrate absorber boundary area), which for the considered parameters is ~1 μs, i.e. $>>\tau_{signal}$. This causes the signal bandwidth to be much larger than the substrate noise bandwidth, so that devices can be deposited directly on the substrates.

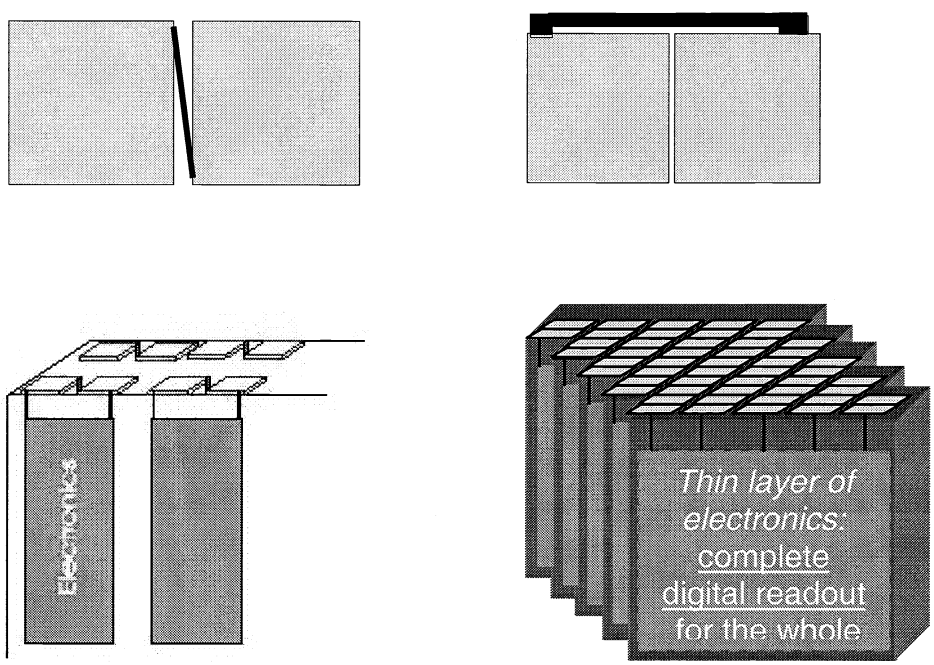

Figure 14. Instead of "pop-up" structures [9], thermoelectric design allows much more rugged pixel array construction: single units (two possible options shown at top) are deposited on the edges of thin substrates, while the electronics is deposited on the larger side of the substrate (left bottom figure). Substrates, each with two rows of pixels, are then stacked into a megapixel array ("book" structure, right bottom figure).

suitable for the QVD detector has been estimated to occupy about 50,000 μm^2, and the remaining circuitry (trigger, multiplexing, storage, and readout) should occupy no more than an additional 50,000 μm^2. The 500 sets of electronics required would then need 10 cm^2 total, which is a wafer 2 x 5 cm. Of course, smaller arrays place fewer demands on the

packaging technology, and the megapixel array is considered a desirable goal. For the individual wafers, some details are already being studied. For instance, single-crystalline silicon substrates of 20 micron thickness are commercially available, and are a good choice because standard niobium processing for superconducting electronics on Si substrates can be utilized. Critical technology development tasks will include sensor device fabrication on the polished edges of such substrates (laser processing is a leading candidate technology for this task), and handling techniques for the fragile wafers during electronics circuitry fabrication. Once the wafers are stacked and bonded, the detector assembly should be quite rugged.

ACKNOWLEDGEMENTS

This work was supported by basic research funding from NRL/ONR, NSF and by NASA Supporting Research and Technology funding.

REFERENCES

1. D.Van Vechten, K. S. Wood, G. G.Fritz, J. S. Horwitz, R. M.Stroud, R. C. Y. Auyeung, J. Kim, S. B. Qadri, A. L.Gyulamiryan, V. R.Nikogosyan, and A. M.Gulian, Studies of anisotropic thermoelectricity in layered oxide materials and time-resolved phonon kinetics, *Physica B* **263-264**, pp. 617-620, 1999.
2. A. M. Gulian, D. Van Vechten, K. S. Wood, G. G. Fritz, J. S. Horwitz, M. S. Osofsky, J. M. Pond, S. B. Qadri, R. M. Stroud, J. B.Thrasher, V. O. Vartanyan, A. S. Kuzanyan, V. R. Nikogosyan, and A. L. Gyulamiryan, Imaging detectors based on the response of anisotropic layered materials, *IEEE Trans. Appl. Supercond.,* **9**, pp. 3194-3197, 1999.
3. B. W. Roberts, Survey of Superconductive Materials and Critical Evaluation of selected Properties, *J. Phys. Chem. Ref. Data*, **5**, pp. 581-821, 1976.
4. A. Gulian, K. Wood, G. Fritz, A. Gyulamiryan, V. Nikogosyan, N. Giordano, T. Jacobs, and D. Van Vechten, X-ray/UV single-photon detectors with isotropic Seebeck sensors, *NIMA* , **444**, pp. 232-236, 2000.
5. D. Van Vechten, K. Wood, G. Fritz, A. Gyulamiryan, V. Nikogosyan, N. Giordano, T. Jacobs, and A. Gulian, Thermoelectric Single-Photon Detectors: Isotropic Seebeck Sensors, in: *Proc. 18-th Int. Conf. On Thermoelectricity* (ICT-99), pp. 477-480, Baltimore, 1999.
6. Innovative products, DUPVA gain amplifier, *Photonics Spectra*, **33**, Issue 33, p. 156, 1999.
7. D. K. C. MacDonald, W. B. Pearson, and I. M. Templeton, Thermo-Electricity at Low Temperatures,*Proc. Roy. Soc.* **A 266**, pp. 161- 184, 1962.
8. N. E. Bickers, D. L. Cox, and J. W. Wilkins, Thermodynamic, Transport, and Excitation Properties of Ce Impurities in a Model Metal: Kondo Resonance and Universality in Mixed-Valence Regime, *Phys.Rev. Lett.*, **54**, pp. 230-233, 1985.
9. C. K. Stahle, S. R. Bandler, T. Barbee Jr., J. Beeman, R. P Brekosky, B. Cabrera, M. Cunningham, S. Deiker, E. Figueroa-Feliciano, F. M. Finkbeiner, M. Frank, K. C. Gedreau, E. E. Haller, G. C. Hilton, K. D. Irwin, R. L. Kelley, S. E. Labov, M. J. Li, N. Madden, J. M. Martinis, D. McCammon, S. Nam, F. S. Porter, H. Schnopper, E. H. Silver, A. E. Szymkowiak, G. S. Tucker, A. Walker, D. A. Wollman, Toward a 2eV microcalorimeter x-ray spectrometer for Constellation-X, *Proc. SPIE*, **3765**, pp. 82-91, 1999.
10. P. B. Johnson and R. G. Goodrich, Anisotropy of the Electron-Phonon Collision Frequency on the Fermi Surface of Silver, *Phys. Rev. B* **14**, pp. 3286-3295, 1976.
11. T. L. Ruthruff, C. G. Grenier, and R. G. Goodrich, Electron-Electron Scattering in Transition Metals, *Phys. Rev. B* **17**, pp. 3070-3073, 1978.
12. C. A. Steele and R. G. Goodrich, Anisotropy of Electron-Phonon Scattering in Gold, *Phys. Rev. B* **24,** pp. 5576-5582, 1981.
13. T. C. O'Hara, P. Broussard, and R. G. Goodrich, Electron-Phonon Scattering in Antimony: RFSE, *J. Phys. F: Metal Phys.,* **12**, pp. 67-77, 1982.
14. C. Kittel, *Introduction to Solid State Physics,* 4th Edition, J. Wiley & Sons, New York, 1971.
15. D. A. Papaconstantopoulos, *Handbook of the Band Structure of Elemental Solids,* Plenum Press, New York, 1986.
16. Handbook of Chemistry and Physics (CRC), 76th Edition, CRC Press, 1996.